

# YALE PEABODY MUSEUM

P.O. BOX 208118 | NEW HAVEN CT 06520-8118 USA | PEABODY.YALE. EDU

## JOURNAL OF MARINE RESEARCH

The *Journal of Marine Research*, one of the oldest journals in American marine science, published important peer-reviewed original research on a broad array of topics in physical, biological, and chemical oceanography vital to the academic oceanographic community in the long and rich tradition of the Sears Foundation for Marine Research at Yale University.

An archive of all issues from 1937 to 2021 (Volume 1–79) are available through EliScholar, a digital platform for scholarly publishing provided by Yale University Library at <https://elischolar.library.yale.edu/>.

Requests for permission to clear rights for use of this content should be directed to the authors, their estates, or other representatives. The *Journal of Marine Research* has no contact information beyond the affiliations listed in the published articles. We ask that you provide attribution to the *Journal of Marine Research*.

Yale University provides access to these materials for educational and research purposes only. Copyright or other proprietary rights to content contained in this document may be held by individuals or entities other than, or in addition to, Yale University. You are solely responsible for determining the ownership of the copyright, and for obtaining permission for your intended use. Yale University makes no warranty that your distribution, reproduction, or other use of these materials will not infringe the rights of third parties.



This work is licensed under a Creative Commons Attribution-NonCommercial-ShareAlike 4.0 International License.  
<https://creativecommons.org/licenses/by-nc-sa/4.0/>



# Journal of MARINE RESEARCH

---

Volume 54, Number 6

## Variability and sources of the southeastern Atlantic circulation

by Silvia L. Garzoli<sup>1,2</sup>, Arnold L. Gordon<sup>1</sup>, Vladimir Kamenkovich<sup>1,3</sup>,  
Dale Pillsbury<sup>4</sup> and Christopher Duncombe-Rae<sup>5</sup>

### ABSTRACT

The 1992–1993 Benguela Sources and Transport (BEST) time series provide a quantitative view of the Benguela Current transport and the eddy field crossing 30S, as well as an estimate of the relation between its barotropic and baroclinic components. This is done by a simultaneous analysis of the BEST data derived from inverted echo sounders, pressure sensors, current meter moorings, CTD, and ADCP stations. The analysis of the time series indicates that the annual mean baroclinic transport of the Benguela Current is 13 Sv with a total transport of 16 Sv. Through the combination of instruments the total baroclinic plus barotropic transport of the upper 2600 m was obtained without making any assumption about the level of no motion. Results from this calculation corroborated the assumption that 1000 m as a level of no motion could be used as a fairly good approximation. The stationary flow of the Benguela Current is mostly confined near the African Continent while a transient flow, composed by large eddies shed from the Agulhas retroflection, dominates the western portion of the Benguela Current. In the stationary part of the Benguela Current, both barotropic and baroclinic components are equally important while in the transient part, the barotropic is more substantial. Several rings were observed during the experiment that migrated toward the west. An initial speed of 12 km/day diminished to 6 to 7 km/day at the Walvis Ridge. The water mass source of the Benguela Current includes Indian and South Atlantic subtropical thermocline water; relatively saline, low oxygen tropical Atlantic water; and the cooler, fresher subantarctic water. Changes in thermocline salinity correlate with transport: in general when the northward transport is increasing

1. Lamont-Doherty Earth Observatory, Columbia University, Palisades, New York, 20964, U.S.A.

2. Present address: Atlantic Oceanographic and Meteorological Laboratory, NOAA, 4300 Rickenbacker Causeway, Miami, Florida, 33149, U.S.A.

3. On leave from P. P. Shirshov Institute of Oceanology, Russian Academy of Science, Russia.

4. College of Oceanic and Atmospheric Sciences, Oregon State University, Corvallis, Oregon, 97331, U.S.A.

5. Sea Fisheries Institute, Roggebaai 8012, South Africa.

the thermocline salinity also increases, without a decrease in oxygen. This indicates that the Benguela Current increases in strength by bringing in more subtropical thermocline water. As the Agulhas input is most effective in boosting the salinity of the upper thermocline (the South Atlantic Current water being deficit in salinity relative to the Indian Ocean source) we suggest that the spatial variations in transport are tied to Agulhas water influx, presumably associated with the eddy field.

## 1. Introduction

The southeastern Atlantic is an area of particular interest for inter-ocean exchange and climate-related issues. It is the gateway for Indian-Atlantic Ocean exchange of mass, heat and salt, a process that has been the subject of numerous studies (e.g. Gordon, 1985; Lutjeharms and Cooper, 1996; Lutjeharms and Webb, 1995). Through a process of eddy detachment and associated entrainment from the Agulhas retroflexion, pulses of warm and salty waters enter the Atlantic. It is possible that this interocean exchange forms a link in the conveyor belt global thermohaline circulation (Gordon *et al.*, 1992; Broecker, 1991; Schmitz, 1995). Along with South Atlantic water masses, ocean water advects northward with the Benguela Current, the eastern boundary current of the South Atlantic subtropical gyre.

The origin and transport of the Benguela current have been the objectives of a field program named BEST, Benguela Sources and Transport, that took place from June 1992 through November 1993 (Garzoli *et al.*, 1994a). The main field work consisted of three hydrographic cruises and the deployment of moored instruments: inverted echo sounders (IES), some of them equipped with pressure sensors (PIES) or ambient noise detectors (ANSL), and current meter moorings (CMM).

The first analysis of the large-scale data set (CTD and IES) revealed some important results concerning the origin and transport of the boundary current (Garzoli and Gordon, 1996). Based on the IES results, in the 16 month mean, the Benguela Current transports 13 Sv northward, 50% of which is derived from the central Atlantic (which may be primarily South Atlantic water), 25% comes from the Indian Ocean (primarily Agulhas water) and the remaining 25% is a mixture of Agulhas and tropical Atlantic water. Water mass analysis (Gordon, personal communication) shows that the sources of the Benguela Current include Indian and South Atlantic subtropical thermocline water, the relatively saline, low oxygen tropical Atlantic water introduced by a nearshore poleward flow and the cooler, fresher subantarctic water. The South Atlantic thermocline and subantarctic inflow is derived from the eastward flowing, high latitude link of the South Atlantic subtropical gyre, (Stramma and Peterson, 1989) part of which turns northward into the Benguela Current. The Indian Ocean water is injected into the Benguela Current through the Agulhas eddy shedding and the Agulhas Retroflexion filament processes (Lutjeharms and Van Ballegooyen, 1988; Shannon *et al.*, 1989). A complex stirring effect of contrasting water types is envisioned. Inspection of the South Atlantic Current reveals that it is composed of a blend of South Atlantic subtropical and subantarctic water (Gordon *et al.*, 1992), making its thermocline somewhat less saline than that observed within the central axis of the subtropical regime marking the crest of the South Atlantic subtropical gyre and

northern limit of the South Atlantic Current (Reid, 1989). The Agulhas and Brazil eddies (Gordon, 1981; Gordon *et al.*, 1987; Smythe-Wright *et al.*, 1996; Duncombe-Rae *et al.*, 1996) within the Benguela Current are marked by thermostad, near 16° in the case of the Agulhas eddies and 13°C for Brazil eddies, accompanied by a positive salinity anomaly relative to the surrounding water, a characteristic of an origin within a winter modified mixed layer (Olson *et al.*, 1992).

The southeastern Atlantic is an area of large time and space eddy variability.<sup>6</sup> At the retroflexion, the main stream of Agulhas Current periodically pinches and sheds a ring (Lutjeharms, 1981; Lutjeharms and Gordon, 1987). Agulhas rings can be identified by a large depression of the 10° isotherm usually between 200 and 500 m (Duncombe-Rae *et al.*, 1996).

The Benguela Current flow is not all stationary. At 30S, it consists of a steady flow, mostly concentrated near the coast, and a transient flow that has been assumed to be mainly concentrated in the western side of the current, close to the Walvis Ridge. The statistical properties of the eddy field observed in the Cape Basin and eastern South Atlantic, were examined by Duncombe-Rae *et al.* (1996). Seven anticyclonic rings were encountered during the hydrographic surveys. Two of them were shown to be of Brazil Current origin (Smythe-Wright *et al.*, 1996; Duncombe-Rae *et al.*, 1996). The inverted echo sounders records indicated that a minimum of 4 to 6 eddies, assumed to be of Agulhas origin, entered the Cape Basin per year during the sampled period. The associated anomaly in heat, salt and volume transports are  $3.3 \times 10^{20}$  J per year, 14 to  $21 \times 10^{12}$  kg salt per year, and  $2.6$  to  $3.8 \times 10^6$  m<sup>3</sup> s<sup>-1</sup>. From the BEST current meter data, Pillsbury and Bottero (personal communication) computed several quantities per ring: available heat  $0.33 \times 10^{20}$  J to  $0.501 \times 10^{20}$  J; the excess salt content is  $2.1 \times 10^{12}$  kg to  $3.1 \times 10^{12}$  kg, and the available potential energy is  $2.81 \times 10^{15}$  J to  $3.81 \times 10^{15}$  J. If the number of eddies that enters the basin is 4 to 6, then results are similar to those obtained from the combination of hydrographic and IES data.

Drifter observations of Agulhas rings yield surface velocities which are higher than those derived from deep referenced geostrophic calculations, suggesting the presence of a significant barotropic component of the flow (Olson and Evans, 1986). In addition, the drift of Agulhas rings is altered by the Walvis Ridge (Gordon and Haxby, 1990; Byrne *et al.*, 1995), also suggestive of a bottom-reaching barotropic component of the flow (Clement and Gordon, 1995; Kamenkovich *et al.*, 1996). Based on these factors, measuring both the barotropic and baroclinic components was necessary to achieve the BEST objective. The hydrographic and the IES data were meant to provide a measurement of the baroclinic flow (Garzoli and Gordon, 1996). The addition of pressure gauges, deployed simultaneously with the IES, was aimed to achieve the objective of obtaining the total velocity of the flow (Wimbush *et al.*, 1990).

6. The term eddy is a generic term for different kinds of coherent oceanic variability. In this paper the term eddy is used when the observations do not allow one to determine if the feature observed has been detached from the main flow. The detached coherent formation will be called rings.

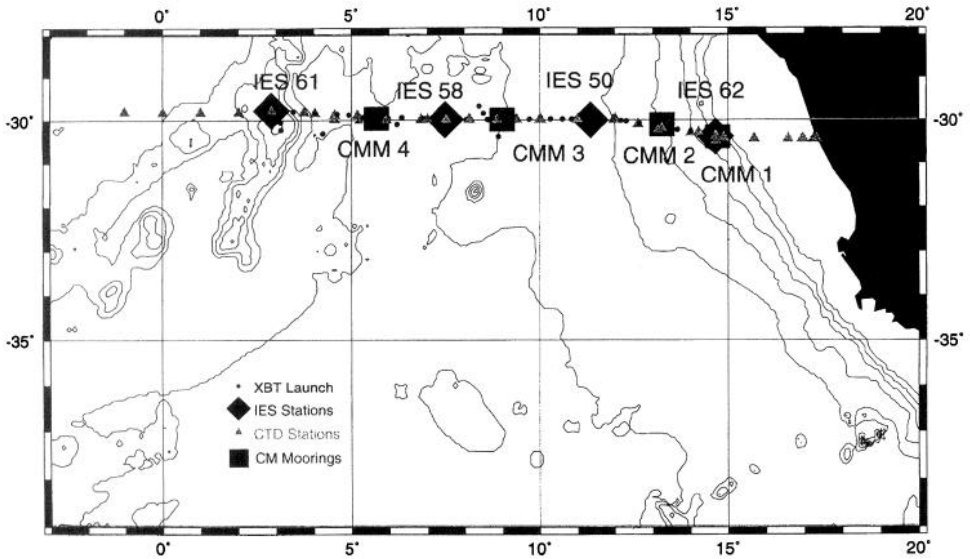


Figure 1. Map with the location of the 3 PIES and the 4 CMM and the location of the CTD stations along 30S.

In this paper, further analysis of the BEST data is undertaken to better resolve the Benguela transport and the eddy field across 30S and to provide an estimate of the relation between its barotropic and baroclinic components. This is done by a simultaneous analysis of all the different data sets. The IES data are analyzed to determine the variability of the baroclinic flow between the three realizations obtained during the BEST cruises. Temperature sensors deployed at the CMM sites are used to increase the zonal resolution of the dynamic height variability obtained from the IES travel time series. Data collected with the pressure gauge sensors deployed simultaneously with the IES are used to determine the variability of the barotropic component of the flow. CMM data provide measurements of the total velocity and its variability to be compared with that obtained by indirect measurements (IES/PIES). Finally, a discussion of the whole BEST data set is given and the main results from the program summarized.

The data analyzed in this paper consist of the following:

—Hydrography: CTD stations collected along 30S between 14°43'E and 1E. These comprise 16 casts obtained during BEST 1 (6/17/92 to 6/25/92); 21 casts during BEST 2 (5/8/93 to 5/14/93), and 12 casts during BEST 3 (10/25/93 to 11/4/93) (Fig. 1). (See data reports: van der Berg, 1992 and Belinne *et al.*, 1996).

—Moorings: Inverted echosounders (IES) equipped with pressure sensors (PIES) and a subset of data obtained with the current meter moorings (CMM) deployed along 30S. Information on the deployment sites as well as the data collected are given in Table 1 and Figure 1. Further details can be obtained from the BEST Data Report 1: IES/PIES/ANSL

Table 1. Location of the moored instruments whose data are analyzed in this paper.

Site	Latitude	Longitude	Data available
PIES 61	29°47.28'S	02°52.48'E	Travel Time/Bottom Pressure @2600 m
CMM 4	30°00.19'S	05°59.75'E	210 m Temperature 510 m Temperature 3010 mV, Temperature
PIES 58	30°00.41'S	07°29.81'E	Travel Time/Bottom Pressure @5173 m
CMM 3	29°59.43'S	08°49.78'E	205 m Temperature 505 m Temperature 4950 m V, Temperature
PIES 50	29°59.32'S	11°58.32'E	Bottom Pressure @3941 m
CMM 2	30°16.88'S	13°13.79'E	210 m Temperature 515 m Temperature 3020 mV, Temperature
PIES 62	30°39.50'S	14°40.13'E	Travel Time/Bottom Pressure @980 m
CMM 1	30°26.65'S	14°42.53'E	215 m Temperature 520 m V, Temperature

(Garzoli *et al.*, 1994b) and BEST Data Report 2: Current Meter Mooring Data (Pillsbury *et al.*, 1994).

—ADCP data: collected during the BEST 2 cruise along 30S (Clement and Gordon, 1995).

## 2. Data analysis, baroclinic component

*a. Dynamic height series.* The baroclinic component of the flow can be determined from the measurements collected with the inverted echo sounders. Garzoli and Gordon (1996) did a first low resolution analysis which determined the mean baroclinic transport of the Benguela Current from the surface to the 1000 m across 30S (for the 16-month period of the observations), as approximately 13 Sv. The procedure followed was to relate the travel time series collected with the IES to corresponding dynamic height obtained from the CTD data using a linear correlation between the two variables. In what follows, the zonal resolution along 30S is improved by analyzing the time series of temperature collected with the current meter moorings at locations between or near the PIES (CMM 4, 3, 2, and 1). This is based on the result that the travel time obtained with the IES is highly correlated to both the dynamic height (Garzoli and Gordon, 1996) and the depth of the 10°C isotherm considered as representative of the main thermocline (Duncombe-Rae *et al.*, 1996). Consequently, the first step is to determine the depth of the thermocline from the temperature sensors and afterward, to relate this depth to the dynamic height. The depth of the thermocline is determined through a linear interpolation of the temperature series collected with the temperature sensors deployed at the current meter sites. A relation

between the depth of the 10°C isotherm and dynamic height is obtained by the analysis of all the CTD casts collected during the program. Details of the procedure are given in Appendix A.

Through the expressions that relate changes in dynamic height to changes in the depth of the thermocline (Appendix A), four series of the variability of the depth of the thermocline and of dynamic height of the sea surface ( $\Delta DH$ ) relative to 1000 m are obtained along 30S at the location of the CMMs. By definition these series have zero mean. The zero mean series are adjusted to D10°C or to dynamic height of the sea surface by recalling the series of the dynamic height values observed with the CTD at the location of the instruments during the three BEST cruises (for details on the procedure see for example, Garzoli and Gordon, 1996). Results are shown in Figure 2 and 3 respectively.

*b. Geostrophic velocities (baroclinic component).* Geostrophic meridional velocities at the sea surface relative to some reference level are obtained from dynamic height values by using the relation:

$$v_g = \frac{g}{f} \frac{\Delta DH}{\Delta x} \quad (1)$$

where  $\Delta DH$  is the difference in dynamic height between stations separated zonally by a distance  $\Delta x$ ,  $g$  is gravity and  $f$  is the Coriolis parameter. Such calculations were done both for the dynamic height values obtained from the CTD data and from the dynamic height series obtained from the procedure described in Appendix A.

While data from the CTD casts provided accurate information about the distribution of the geostrophic velocities with depth (along 30S) at three different snapshots, the series of dynamic height based on IES and CMM data provided the integrated evolution of these fields with time. We call it integrated because no details are given on the vertical structure. The time evolution of the geostrophic velocities obtained from the dynamic height series is given in Figure 4. The statistics of the velocity series are given in Table 2.

*c. Transports.* The meridional velocities obtained using Eq. (1) are the baroclinic components of the total velocity. Corresponding transports are calculated by using the approximation that the geostrophic velocity decreases nearly linearly with depth. Under this assumption, the transports are calculated through the relation:

$$T_r(\text{Sv}) = kV_g\Delta x\Delta z \quad (2)$$

where  $k$  ( $= 0.4$ ) is the empirically determined constant (Garzoli and Gordon, 1996),  $\Delta x$  is the distance between stations, and  $\Delta z$  is the depth of the reference level. By analyzing the vertical profiles of geostrophic velocity and determining the corresponding errors Garzoli and Gordon (1996) proved that this was a valid first approximation. The error was found to be  $\pm 1$  Sv and the values so calculated interpreted as the lower limits. In what follows,

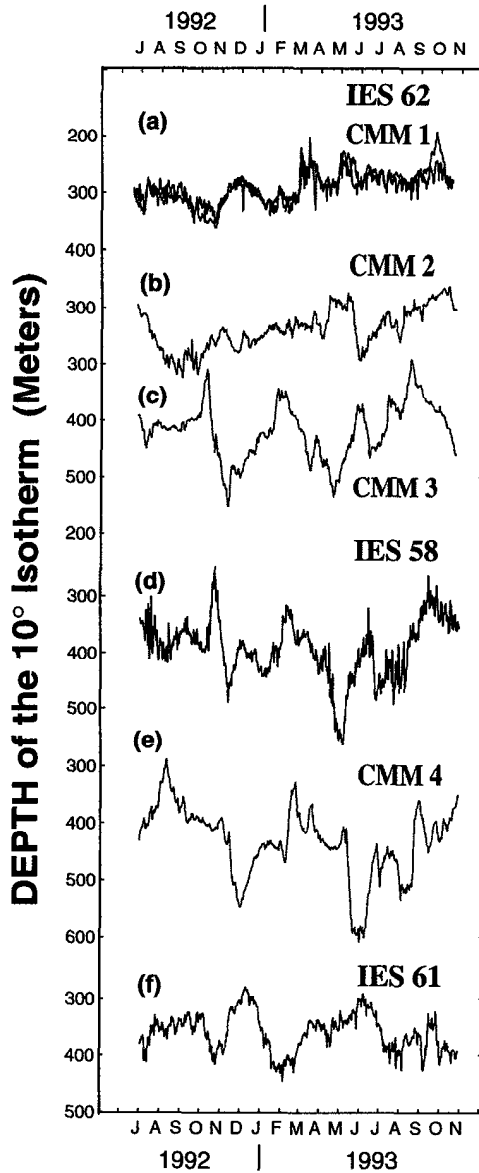


Figure 2. Series of the depth of the 10°C isotherm along 30S at latitudes: (a) 14° 40.13'E and 14° 42.53'E; (b) 13° 13.79'E; (c) 08° 49.78'E; (d) 07° 29.81'E; (e) 05° 59.75'E; (f) 02° 52.48'E.

similar calculations will be done for the new series of geostrophic velocities, and results will be compared with those obtained from hydrography.

The transport series across 30S are given in Figure 4 (right scale), and the corresponding statistics, in Table 3. To validate these series, the transport values obtained are compared



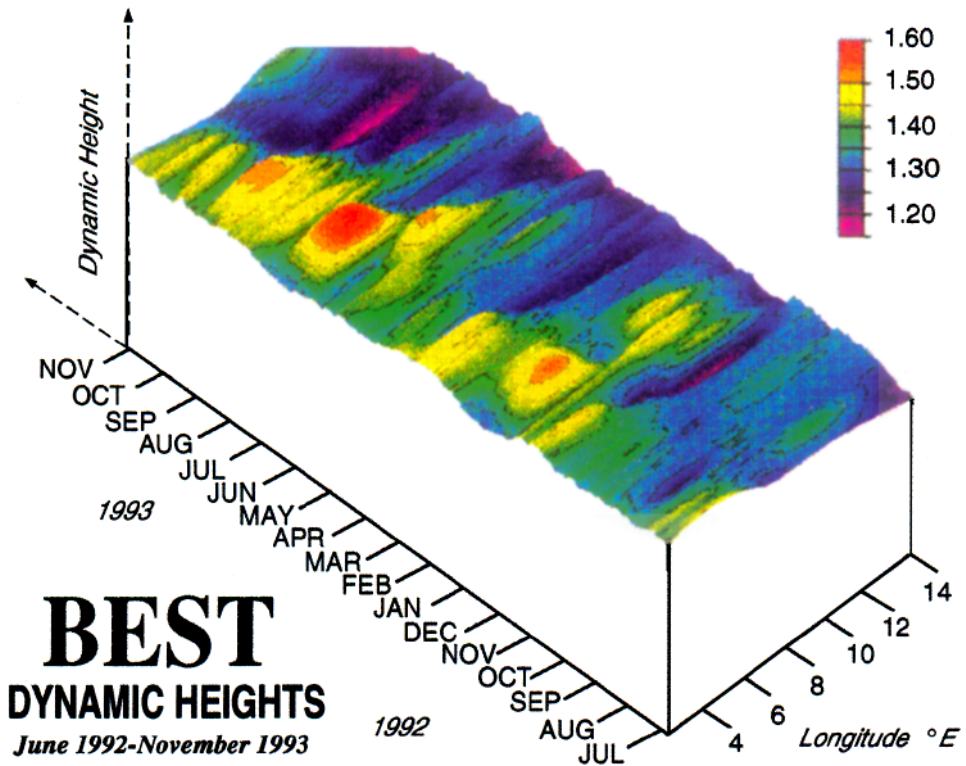


Figure 3. Time-latitude variability of dynamic height of the sea surface relative to 1000 m across 30S derived from the BEST time series.

with those derived from the CTD stations data. Figure 5 shows the integrated (from the African coast) transports calculated from the CTD casts during the 3 BEST cruises as a function of longitude. Superimposed (circles) are the values obtained from the dynamic height series. It must be noted that only the comparison made for BEST 2 is done at the exact dates. For the other two cruises, there is a difference between the starting or ending dates of the series and the dates in which the CTD data were collected. This is due to two factors: even though the calibration to dynamic height is done with the hourly data (i.e., CTD and dynamic height variability are measured the same day and hour), to calculate transports from differences in dynamic height the files need to be cut to the same length. In this way, several days are lost at the beginning and end of the records. Moreover, in the case of BEST 3, three days of data at the end of the IES 62 record were lost; in this case the comparison between CTD and IES transport data was done between values collected almost 10 days apart. A difference in the first station will translate, by integration, to all the others. For this reason in Figure 5 (BEST 3) the transport between CMM2 and IES 62 during BEST 3 was made equal to the one obtained from the CTD.

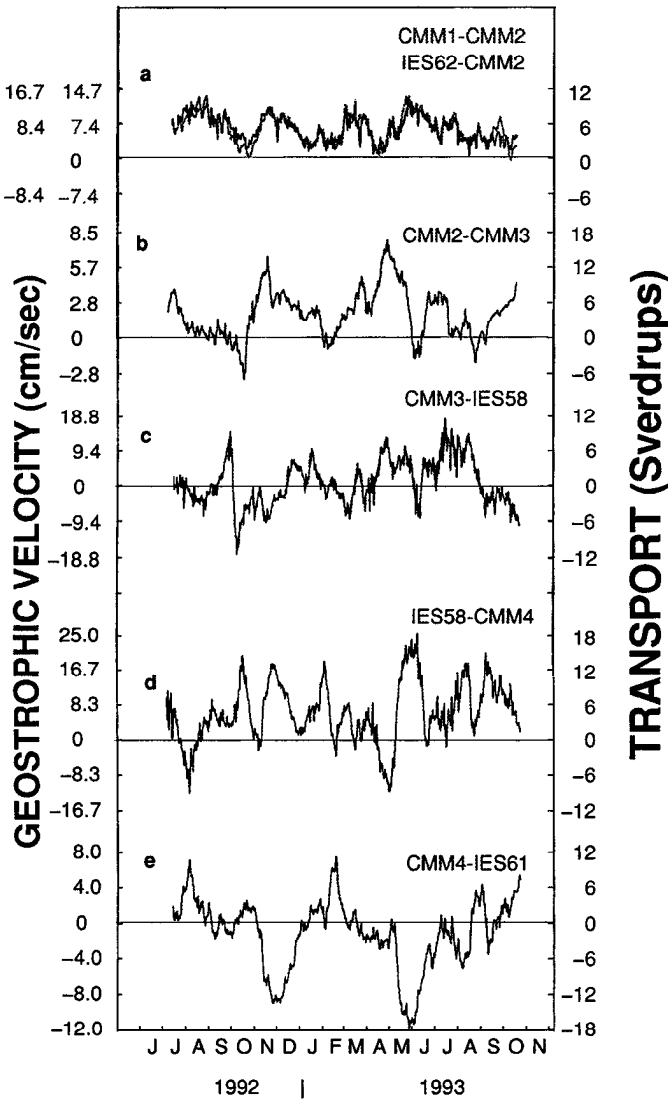


Figure 4. Geostrophic velocities (at the sea surface referenced to 1000 m) and corresponding transports as functions of time along 30S.

To complete the analysis, the series are analyzed by seasons. The results of a simple statistics of the series (maximum, minimum, mean and standard deviation) are given in Table 4. The mean values given in Table 4 are displayed graphically in Figure 6 which compares the results with those previously obtained by Garzoli and Gordon (1996) with less zonal resolution.

Table 2. Statistics on the velocities series shown in Figure 4.

Site	Min	Max	Mean	STD
PIES 62–CMM2	0.32	14.84	7.00	3.08
CMM2–CMM3	–3.29	7.82	1.98	1.96
CMM3–PIES 58	–17.58	18.20	0.55	6.05
PIES 58–CMM4	–12.39	25.38	6.60	6.97
CMM4–PIES 61	–11.88	7.42	–1.02	3.86

Columns are: site, minimum (min), maximum (max), mean (mean) and standard deviation (SD). All values are given in cm/s.

### 3. Discussion of the baroclinic field

Agulhas eddies can be identified in the depth of the 10°C isotherm series as large depressions, usually between 200 and 500 m (Duncombe-Rae *et al.*, 1996). Depressions of these magnitudes are not observed close to the African coast (Fig. 2) but start to become significant at 8° 50'E (location of CMM 3). Figure 2 indicates that the series at 7° 30'E and 8° 50'E (PIES 58 and CMM 3) are very similar. They were obtained at locations separated by 128 km, a distance smaller than the diameter of the observed rings (Duncombe-Rae *et al.*, 1996). They both show depressions of the isotherms of the order of 200 to 300 meters during October–November 1992 and April–May 1993. A lag correlation analysis (not shown) indicates that the series at CMM 3 lag the series at PIES 58 with a period of 10 days. Farther west, at 5° 59'E (CMM 4), a depression of 200 m is observed during May–June (with a lag of 20 days with respect to the eastern location) indicating a westward displacement of the eddies. A second depression of the isotherms is observed between November and December 1992, which is observed again a month later at 2° 52'E. There is no doubt from the lag correlation analysis and the visual observation of the records, that the propagation of one or more features has been observed. If it is assumed that the feature corresponds to a ring and that the same portion of the ring is passing through the deployment site, then it is possible to calculate the velocity of the ring. The distance between stations at 7° 30'E and 8° 50'E (PIES 58 and CMM 3) is 128 km; this indicates that the perturbation moves at a speed of 12.8 km/day or 14.8 cm/s. In a similar way, the velocity of displacement of the rings is 7.2 km/day between stations PIES 58 and CMM 4,

Table 3. Statistics on the transport series shown in Figure 4.

Site	Min	Max	Mean	STD
PIES 62–CMM2	0.23	10.66	5.03	2.22
CMM2–CMM3	–6.97	16.55	4.19	4.16
CMM3–PIES 58	–11.25	11.64	0.35	3.87
PIES 58–CMM4	–8.93	18.29	4.75	5.02
CMM4–PIES 61	–17.88	11.17	–1.54	5.80

Columns are: site, minimum (min), maximum (max), mean (mean) and standard deviation (SD). All values are given in Sv (1 Sv = 10<sup>6</sup> m<sup>3</sup>/sec).

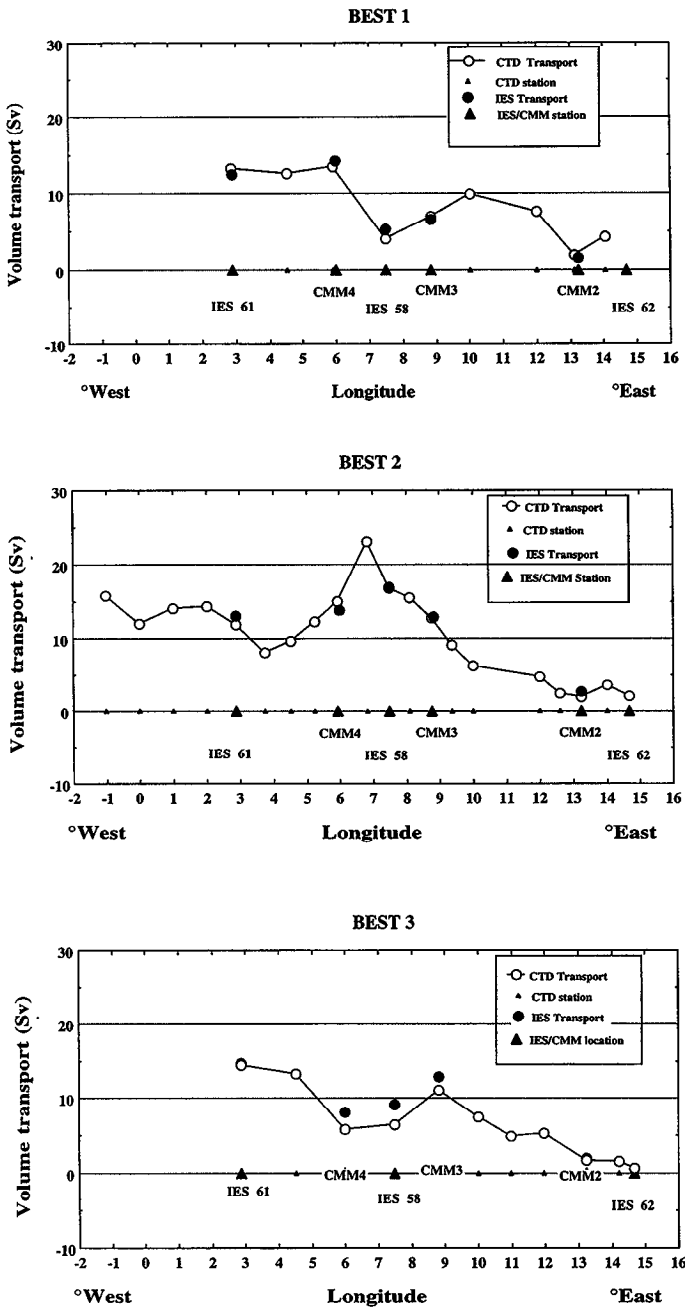


Figure 5. Comparison between the baroclinic transports obtained from the dynamic height/ geostrophic velocity series and those from the CTD casts during (a) BEST 1; (b) BEST 2 and (c) BEST 3. Transports are calculated for reference level 1000 m and integrated from the coast.

Table 4. Seasonal Transports in Sverdrups

Site	Winter 92				Spring 93				Summer 93				Fall 93				Winter 93			
	Min	Max	Mean	SDev	Min	Max	Mean	SDev	Min	Max	Mean	SDev	Min	Max	Mean	SDev	Min	Max	Mean	SDev
CMM1-CMM2	-0.6	10.1	6.0	2.6	0.5	8.5	4.9	2.4	1.4	10.1	4.3	2.0	0.6	10.9	5.8	2.7	2.0	8.0	4.6	1.6
IES62-CMM2	0.3	10.7	6.8	2.4	1.4	8.8	5.5	1.9	1.0	8.2	4.1	1.8	0.5	9.6	5.3	2.4	0.2	7.5	4.3	1.5
CMM2-CMM3	-1.3	8.3	2.3	2.4	-7.0	13.8	4.3	4.8	-1.9	10.5	3.5	2.8	-3.5	16.5	7.1	5.2	-4.2	7.8	2.5	2.9
CMM3-IES58	-8.1	2.2	-1.7	1.9	-11.3	9.3	-2.0	3.9	-5.5	6.4	0.7	2.6	-5.4	8.4	2.2	3.1	-5.3	11.6	3.7	3.7
IES-58-CMM4	-8.9	8.3	1.6	3.8	-1.8	14.6	6.4	4.1	-2.6	13.5	3.9	3.2	-8.8	18.3	4.4	7.7	-1.1	14.9	6.3	4.0
CMM4-IES61	-2.6	10.7	2.7	2.8	-13.5	3.9	-4.0	5.9	-7.7	11.2	1.5	3.9	-17.9	0.7	-7.0	5.9	-7.7	6.5	-2.0	3.7

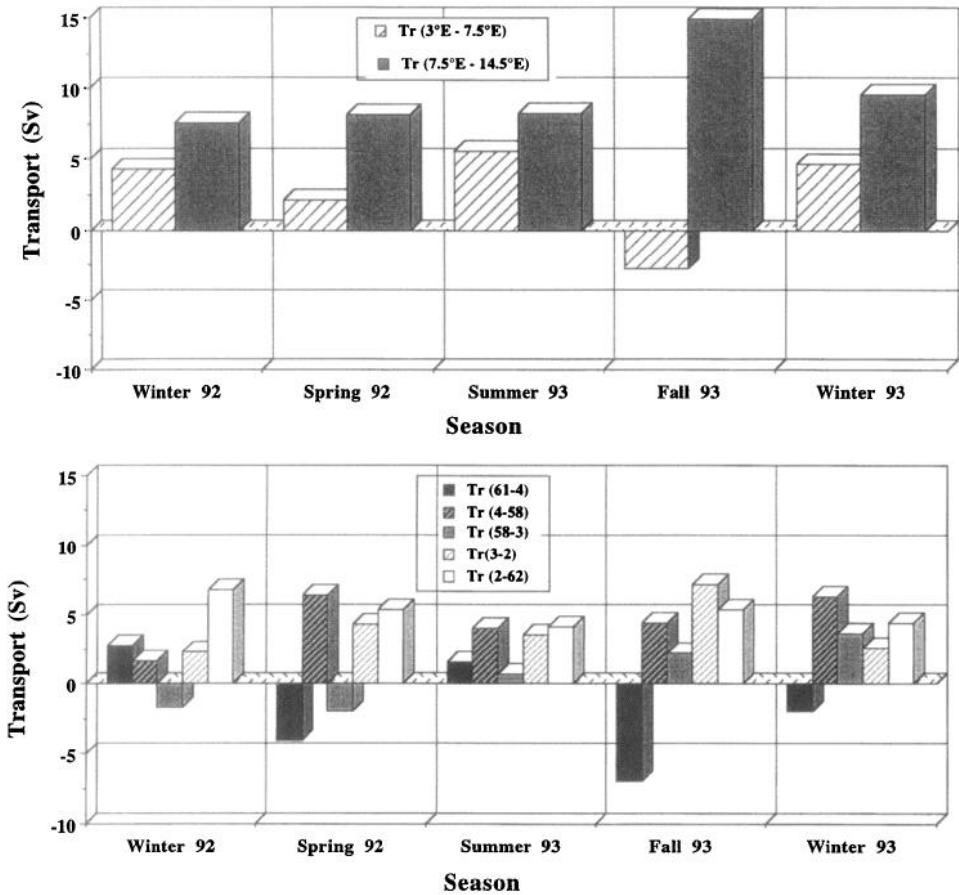
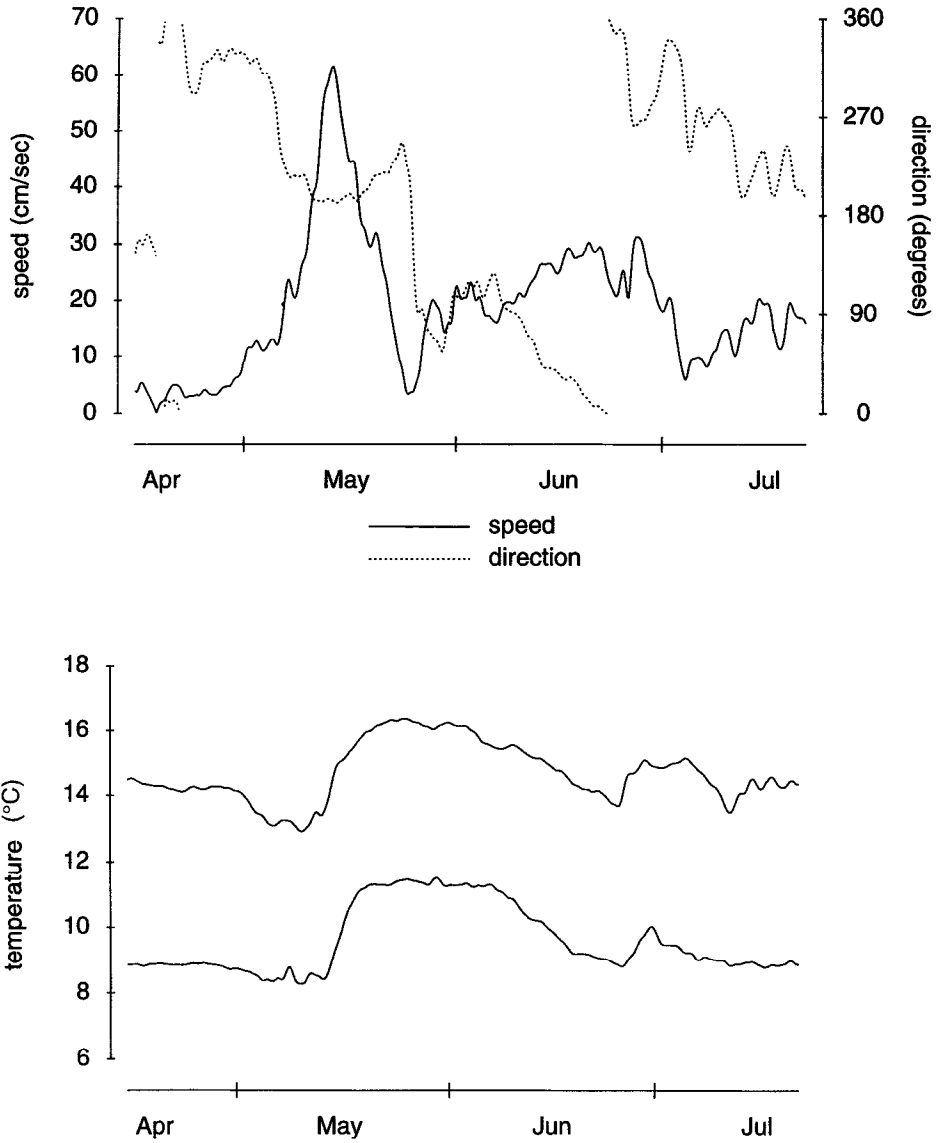


Figure 6. Baroclinic transports by season. Top panel, with low resolution, adapted from Garzoli and Gordon (1996). Lower panel, each bar indicates the direction and magnitude of the volume transport in Sverdrups between station pairs given in the legend.

and 5 km/day between CMM 4 and PIES 61. The speed of propagation of these rings was also analyzed from the CMM records (Pillsbury and Bottero, personal communication) and results are of the same order of magnitude. Pillsbury and Bottero (personal communication) examined the eddy identified as B2-0 by Duncombe-Rae *et al.* (1996) and analyzed in detail by Clement and Gordon (1995) from the hydrographic and ADCP data. This ring was selected because it passed over two of the BEST current meter moorings, CMM3 and CMM4. One limb of the ring touched CMM3 during April 1993, and the entire ring passed over CMM4 during May and June. At CMM4 the ring followed a course toward the W/NW, and the center of the ring appears to have passed either directly over the mooring or near it. The current meter records show (Fig. 7), that it took about 45 days for the temperature anomaly to pass CMM4. The diameter of the ring was estimated to be 240 km,



1993

Figure 7. Detail on the series of total velocity and direction (top panel) and temperatures at 210 m and 510 m (lower panel) recorded during April through June 1993 at current meter mooring site 4.

then the eddy's translation speed was about 6 cm/s. In these records, the edge of the temperature anomaly coincides with the speed maximum which occurs on 14 May as the ring begins crossing over the mooring. The speeds first begin to rise above ambient levels about 12 days earlier. Taking 6 cm/s as the ring's translation speed, this means that the

radius of the speed anomaly is about 62 km greater than that of the temperature anomaly, or equal to 182 km.

No lag correlation at these periods is observed between the records east of 8° 50'E. Byrne *et al.* (1995) tracked rings across the Atlantic from GEOSAT observations, and determined a velocity of translation of 1 to 5 km/days (1 to 7 cm/s) west of the Walvis Ridge. In our opinion these values, lower than the ones obtained in this paper, indicate that the rings are far more energetic after detachment from the main flow. In their motion across the Atlantic, they lose energy and their velocity decreases.

Duncombe-Rae *et al.* (1996) observed a recoil effect in which the thermocline appears to shallow considerably after the passage of an eddy before relaxing to the local mean at 7° 30'E (PIES 58). It is interesting to note that this effect is also observed and is even more pronounced at 8° 50'E (CMM 4). This recoil effect can be attributed to the fact that an anticyclonic ring is usually accompanied by a smaller cyclonic vortex as has been shown by McWilliams and Flierl (1979) and Mied and Lindemann (1979). Observations made by Hooker and Brown (1994) in the Gulf Stream tend to confirm this result as well.

The variability of the baroclinic field across 30S is clearly displayed in Figure 3 which shows the surface dynamic height (relative to 1000 m) as a function of longitude from the Walvis Ridge (2E) to the African coast (14E). In this figure the eddy corridor is clearly distinguished between 2 and 8E. Eddies are depicted as hills in the dynamic height. They are mostly concentrated in the western side of the section. On the eastern side of the section the flow is more steady. Thus, the transient flow associated with the Benguela Current is concentrated near the Walvis ridge while the steady part of the flow is located between the African coast and 8E.

By looking at Figure 3, four main rings crossing 30S can be counted. In a more quantitative way, the autocorrelation analysis of the series in the western side of the section shows a significant peak between 130 and 145 days, indicating the passage of 4 rings during the recorded period. Duncombe-Rae *et al.* (1996) indicated in their study that a minimum of 4 to 6 rings enter the Cape Basin area. The present results show also that for the same period of time as that analyzed by Duncombe-Rae *et al.* (1996) about four eddies made their way into the Atlantic across 30S between the Walvis Ridge and the African coast. This suggests that only one third of the rings that are detached from the Agulhas retroflection deviates toward west, south of the Walvis Ridge.

Another result from the autocorrelation analysis between the series along 30S is that the series at the edge of the shelf (PIES 62 and CMM 1) have significant peaks for a period of 100 to 110 days. This is interpreted as a seasonal signal that can be observed in the records collected in shallower waters. The variability observed in dynamic height across 30S translates to changes in the velocity and transports fields.

In the eastern side of the section (Fig. 4, a and b) the velocities always remain toward the north for almost all the period. Close to the coast the velocity series indicates a variability with a period between 3 and 4 months which may be indicative of seasonality in the transport of the Benguela Current. At this location, there are no abrupt changes due to eddy variability and a seasonal signal is due to the proximity of the coast (or shallow waters). In



the center of the section, between CMM 2 and 3 (Fig. 4c) the variability is less pronounced (standard deviation,  $S_D = 1.26$  cm/s), indicating a steady flow. The largest variability is observed due to the passage of rings in the westward side of the section (Fig. 4c, d, e). Maximum northward velocities are observed between PIES 58 and CMM 4 (25.4 cm/s) during May–June 1993 and associated with the shear of the May 93 ring. The comparison between the transports obtained from data collected with the IES and those collected with CTD casts made during the three BEST cruises (Fig. 5) indicates that the methods applied are correct. The agreement is very good.

The mean total transport across 30S (between  $8.5^\circ$  and  $13.12^\circ$ ) for the upper kilometer is in agreement with the previous result of 13 Sv (Garzoli and Gordon, 1996; Table 3). The only difference is the distribution of this transport across the section. The new resolution allows us to determine that in the mean, northward flow occurs between the African coast and 6E. Mean southward flow is restricted to the part of the section between 3 and 6E (CMM4 and PIES 61). When transports are analyzed by season, it can be noted that east of  $13E$ , the flow is northward all year long, confirming previous results which indicated that, with rare exceptions, the stationary part of the Benguela Current flows toward the north at this location.

The low resolution analysis (Garzoli and Gordon, 1996) indicated that the two winters observed were very similar. This result is valid for the zonal mean, but the present higher resolution analysis indicates differences that previously were not resolved. While during the winter of 1992 the flow between the western stations (Tr (61-4) Fig. 6) is northward, it is toward the south a year later. This can be explained by the passage of rings. During August 1993 a ring was moving north at this location. It can be observed in the dynamic height variability (Fig. 3) as well as in the transport series (Fig. 4). If such rings have some periodicity as it has been suggested, and there is a persisting “recoil” phenomenon in the area described above, then it is to be expected that an eddy passed the region during May/June 92, before the series started. The northward flow observed during the winter of 92 in the transport series between locations CMM4 and IES 61 would then be the result of the “recoil” effect. The two large eddies observed on November/December 92 and May/June 93 are the cause of the significant southward flow observed at this location during the spring 92 and fall 93. In the center of the analyzed section, between longitudes  $8.5$  and  $13.12E$ , the flow is northward during the winter and spring of 1992 and northward during summer, fall and winter 93.

The IES data clearly reveal variability of the Benguela Current transport (Garzoli and Gordon, 1996; Table 4, Fig. 4). Does the ratio of the potential source water vary in concert with transport? The answer seems to be yes. The three BEST CTD transects along 30S reveal variations in the upper thermocline salinity (at  $15^\circ C$ ) versus longitude which are likely to reflect changes in the ratio of the contribution of the various Benguela source waters. To further look into this relation, the transport across 30S is compared with the thermocline salinity (Fig. 8). The changes in thermocline salinity correlate with transport [correlation coefficient ranges from 0.60 to 0.81]: in general, when the northward transport

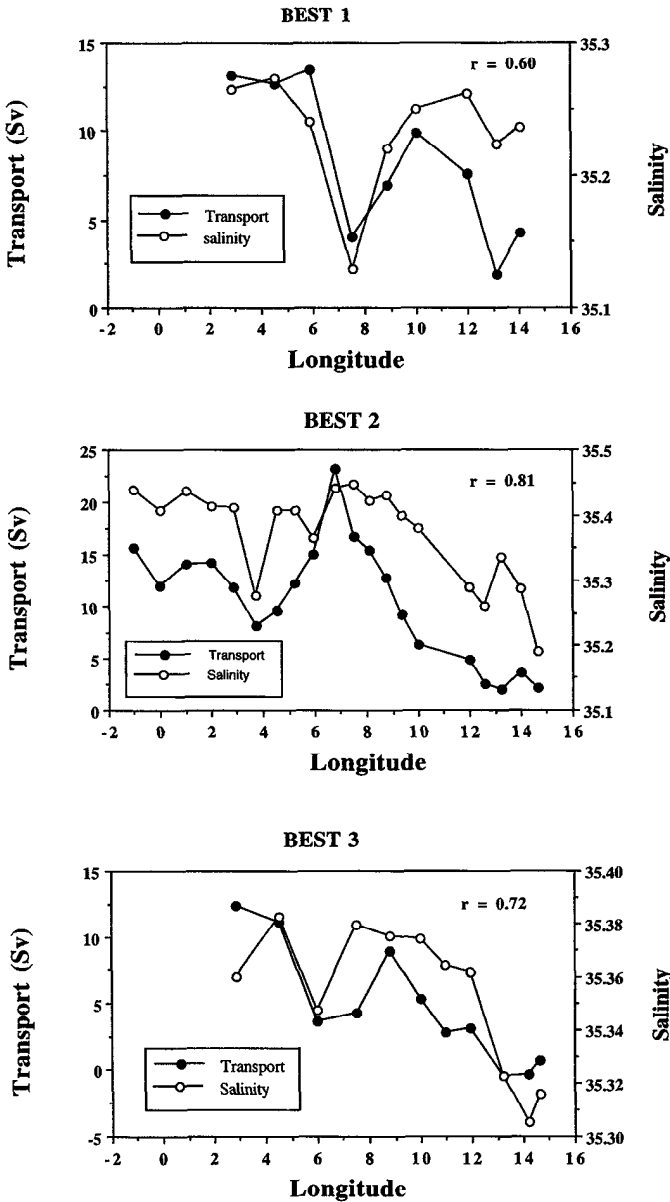


Figure 8. Comparison between salinity at the thermocline level and integrated transport along 30S for the three BEST cruises (from top to bottom, BEST 1, 2 and 3). The coefficients of correlation between the two curves are 0.61, 0.81 and 0.72 respectively.

is increasing (on moving westward along the section) the thermocline salinity also increases. This indicates that the Benguela Current increases in strength by bringing in more subtropical water. As the Agulhas input is most effective in boosting the salinity of the upper thermocline (the South Atlantic Current water being deficit in salinity relative to the Indian Ocean source), we suggest that the spatial variations in transport are tied to Agulhas water influx, presumably associated with the eddy field.

In addition to the salinity-transport correlation, there is a more general shift of thermocline salinity values: for BEST 1 the overall salinity of the upper thermocline is less than that observed during BEST 2 and 3. While Agulhas eddies still seem to influence the distribution form of the transport versus longitude across the Benguela Current, it is likely that during BEST 1 there was an increased relative influx of South Atlantic Current water.

Thus, the BEST data suggest that the source of the Benguela Current may change spatially and temporally as the ratio of potential source waters changes. These issues will be developed further in a detailed water mass analysis study, but this preliminary assessment clearly reveals changes in the blend of source waters for the Benguela Current during the course of the BEST experiment, which may act in concert with transport variability.

#### 4. Data analysis, total velocity

*a. Total geostrophic velocities.* At the four PIES locations along 30S pressure was measured as a function of time in addition to the travel time series. The corresponding series are shown in Figure 9. The series has been de-trended and filtered to eliminate the time-mean and periods lower than two days. It may be noted that at PIES 50 the record is shorter. This is due to a malfunction of the instrument at the beginning that corrected itself during October 2.

Combining data collected with the PIES (travel time and pressure), the variability of the total geostrophic velocity  $v_g$  can be obtained (Chiswell *et al.*, 1986, 1987). The variable part of the *baroclinic component* of the total velocity can be derived from the IES records of travel time as it was done before. In this case 2600 m was chosen as a reference level to calculate the geostrophic velocities between stations. This depth was chosen for the following reasons: (1) the time-variability below 2600 is negligible (see Appendix B), and (2) comparisons between CTD stations taken very close but offshore (deeper depth) of the shallow deployment (PIES 62) indicate that all the variability in dynamic height is in the upper 1000 m and that this variability is similar to that obtained a few meters off shore where the depth is 2600 m. PIES 62 was deployed at the edge of the continental shelf and therefore the variability observed in this record is representative of the variability of dynamic height up to 2600 m. On the basis of this result, time series of geopotential anomaly ( $\Phi$ ), referenced to 2600 m, were obtained and from those series, the variable part of the baroclinic component of the total geostrophic velocity  $v_g'^\phi$  was found through the

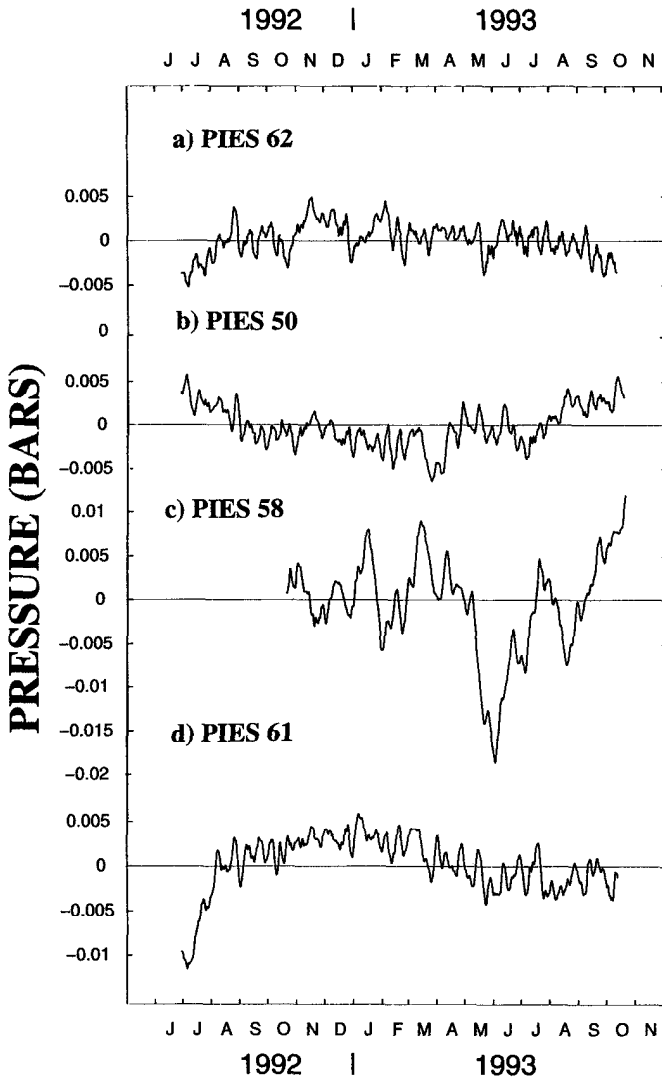


Figure 9. Time variability of the pressure at locations from east to west: (a) PIES 62; (b) PIES 50, (c) PIES 58 and (d) PIES 62. The time-mean of the series has been subtracted.

relation:

$$v'_g \phi = \frac{1}{f} \frac{\Delta \Phi'}{\Delta x} \tag{3}$$

where  $\Delta \Phi'$  is the difference in the time variable part of geopotential anomaly  $\Phi'$  between 2 stations separated by a distance  $\Delta x$ .

The errors incurred in this calculation depend on the error of the estimate of dynamic height from travel time which, in this case, is  $\epsilon = \pm 0.0274$  dyn m. This error yields an error in the velocities that varies from 0.3 to 0.5 cm/sec (Garzoli and Gordon, 1996).

The variable part of the *barotropic component*<sup>7</sup> of the total velocity can be calculated by measuring the difference in pressure between two stations separated by a distance  $\Delta x$ . The depths of the deployments are not important because the time mean of the records was removed and all that is left is the variability, independent of depth (see Appendix B). Therefore, from the differences in the variable part of pressure  $p'$  between two locations separated by a distance  $\Delta x$ , the variable part of the barotropic component of the geostrophic velocity  $v'_g{}^p$  can be obtained from

$$v'_g{}^p = \frac{1}{\rho_0 f} \frac{\Delta p'}{\Delta x}. \quad (4)$$

In this case the error depends on the accuracy in measuring the difference in pressure. Errors in pressure depend on two factors: the first one is the absolute accuracy of the mean pressure, which is 0.015% of 10,000 psi or 1.5 db. The absolute accuracy is not an issue here because the depth of the instruments is unknown and the means have been removed. The second one is the error in removing the drift of the records. It is estimated that the de-drifted records have less than 0.02 db of uncertainty for records at least one year long. This yields an error in the velocities that varies from 0.3 to 0.4 cm/s. Errors of this magnitude can translate into large error in transport but as we will see later, these errors are less than 10% of the total signal.

Thus the variable part of the total geostrophic velocity is given by:

$$v'_g(t) = v'_g{}^\phi + v'_g{}^p \quad (5)$$

where the first term is the variable part of the geostrophic velocity due to the differences in geopotential anomaly (referenced to 2600 m) and the second term is due to differences in pressure at the reference level of 2600 m. Both quantities have zero mean. To determine the mean to be added to obtain the total geostrophic velocity, two different methods are applied. In method 1, both terms on the right-hand side of Eq. (6) are scaled separately using hydrographic and current meter data respectively. In method 2, the left-hand side term of Eq. (5) is adjusted to the total velocity measured by board mounted ADCP (up to 248 m) between the PIES moorings.

*b. Method 1.* 1. The CTD data collected during cruises BEST 1, 2 and 3 are used to calculate the geostrophic velocity (between stations obtained at the location of the deployments) referenced to 2600 m. These values are used to adjust the values of the

7. The definition of the baroclinic and barotropic component of the velocity differs from paper to paper. We call the total velocity at some level chosen for convenience, as the barotropic component. The difference of the total velocity and so defined barotropic component is called the baroclinic component.

variable part of the baroclinic component of the velocity,  $v'_g{}^\phi$ . Thus the baroclinic component of the geostrophic velocity,  $v_g{}^\phi$ , (referenced to 2600 m) is obtained by:

$$v_g{}^\phi = v'_g{}^\phi + K \quad (6)$$

where  $K$  is derived from the adjustment to the CTD data. This procedure does not increase the errors. If anything, errors decrease because the series are adjusted in three points to the measured dynamic height. This is done for  $v_g{}^\phi$  between station pairs (61-58) and (58-62) only (see Fig. 1 for locations) because the travel time record at station PIES 50 was unfortunately lost.

2. Current meter moorings were deployed between the PIES. These moorings contained current meters deployed at a depth of approximately 3000 m. If it is assumed that the total geostrophic velocity at 2600 and 3000 m are (approximately) the same, we can represent the total geostrophic velocity at 2600 m (barotropic component) as:

$$v_g^p = v'^p + \bar{v}_{cmm} \quad (7)$$

where  $v'^p$  is the variable part of the barotropic component derived from the pressure sensors and  $\bar{v}_{cmm}$  is the time-mean velocity recorded by the current meters.

The error in this procedure is the error in the assumption. If the assumption is good, then results from method 1 and 2 should coincide within the limits of the estimates. This procedure is applied for station pairs PIES 61 and 58 (using CMM4 data); 58 and 50 (using CMM3 data), and 50 and 61 (using CMM2 data) (see Fig. 1 for locations).

3. The total velocity is therefore the sum of the terms given by (6) and (7).

$$v_g^{T1} = v_g^p + v_g{}^\phi \quad (8)$$

where the subscript  $T_1$  means total velocity and method 1.

*c. Method 2.* In this method baroclinic and barotropic components are not considered separately. To calculate the mean of the total velocity, ADCP data collected along 30S during BEST 2 (Clement and Gordon, 1995) are used. These data provided the components of the total velocity in the upper layer (up to 258 m). Thus, at the sea surface

$$v_g^{T2} = v'_g(t) + \bar{v}_{ADCP(t_1, t_2)} \quad (9)$$

where  $v'_g$  is calculated by (5) and  $\bar{v}_{ADCP(t_1, t_2)}$  is the mean velocity as measured with ADCP between  $t_1$  and  $t_2$ . The superscript  $T_2$  means total velocity and method 2.

The error committed in this procedure is the error of the ADCP measurements, which, according to Clement and Gordon (1995), is from 1 to 2 cm/s.

This method was applied to station pairs: PIES 61 and 58, PIES 58 and 62, and PIES 61 and 62. As mentioned before, at PIES 50, the travel time record was lost. Therefore, only the barotropic component of the geostrophic velocity was obtained. Also, the beginning of the pressure record at station 58 was useless. Therefore, and because of the need to have

series of the same length in order to obtain differences, all series were cut to the start of the PIES pressure good record, that is, October 1992.

Comparison of results from different methods gives an additional estimate of the validity of the assumptions. Also, total transports obtained between PIES 61 and 62 should coincide with the sum of the transports between the individual station pairs. Results are shown in Figures 10, 11 and 12. The total velocities at the sea surface obtained by the two different methods are very similar, which lead us to believe the validity of the procedures. A comparison of the statistics of the total velocities obtained by the different methods is given in Table 5.

Once we are satisfied with the geostrophic velocities at the sea surface and at the reference level of 2600 m, then the total transports can be obtained. This was done with a method similar to that applied in the first part of this paper, i.e. by assuming an approximately linear decrease of the velocity with depth with the difference that a new constant of proportionality for Eq. (2) needs to be obtained now. The analysis of 30 CTD deep stations obtained along 30S yields a value of  $k = 0.3$  for reference level 2600 m. The standard error is  $\pm 0.02$  and the variance 0.01. Results are given in Table 6 that show graphically the method applied and the mean total transports obtained. All transports are mean values for a year of observations. An explanation of columns and rows in Table 6 is as follows:

Method 1: The first row indicates the baroclinic transport  $T_r^\phi$  from the surface to 2600 m. It is obtained by assuming that the baroclinic component of the total velocity decreases almost linearly from its value at the surface to the reference level 2600 m (area shaded in column 2). The value used for the constant of proportionality  $k$  is 0.3. In this way the mean transport obtained between stations (58-61) (column 3) is 11 Sv and between stations (62 and 58) is 25 Sv.

The barotropic component of the total transport,  $T_r^p$  (the second row), is obtained as the area of the rectangle formed by the mean barotropic velocity at the reference level used for the calculation of the baroclinic component. Results are  $-10.0$  Sv for station pair (58-61) and  $-11$  Sv for stations (62 and 58). The total transport (the third row) is the sum of the 2 previous estimates and it results in 1 Sv between stations (58-61) and 14 Sv for stations (62-58).

In order to compare with the previous estimates, the total geostrophic velocity at the surface is assumed to decrease linearly down to 1200 m and 1000 m. Results are given in row 4.

Method 2: The total velocity obtained by adjusting the data to the ADCP values is assumed to decrease almost linearly with depth down to a reference level of 1200 and 1000 m (column 2). The mean transport between stations (58-61) is 4.5 and 4.0 Sv and 11.5 and 10 Sv for stations (62-58) (columns 3 and 4). With this method of calculation the total mean transport was calculated between the 2 stations that bracket the Benguela Current between the Walvis Ridge and the South African coast: PIES 62 and 61. The results, 17 Sv for the upper 1200 m and 14 Sv for the upper 1000 m, are given in column 5.

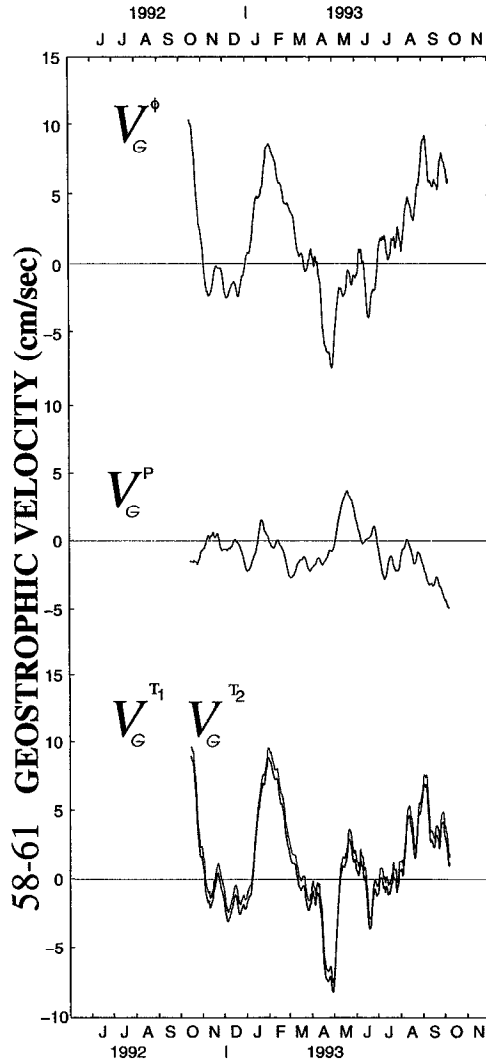


Figure 10. Geostrophic velocity as a function of time for station pairs 61 and 58: (top) baroclinic component of the geostrophic velocities, at the surface referenced to 2600 m, from the difference in  $\Phi$ ; (middle) barotropic component of the geostrophic velocity from the difference in pressure; (bottom) total geostrophic velocity at the surface from method 1 superimposed to the geostrophic velocity from method 2 (thinner line).

## 5. Discussion of the total velocity and transports

The analysis of the results shown in Table 6 indicates that the barotropic component of the flow results in the same transport in the western side of the section (where the eddy corridor is located) as in the eastern side of the section where the steady part of the Benguela Current is observed. In both cases it is  $-10$  to  $-11$  Sv toward the south.



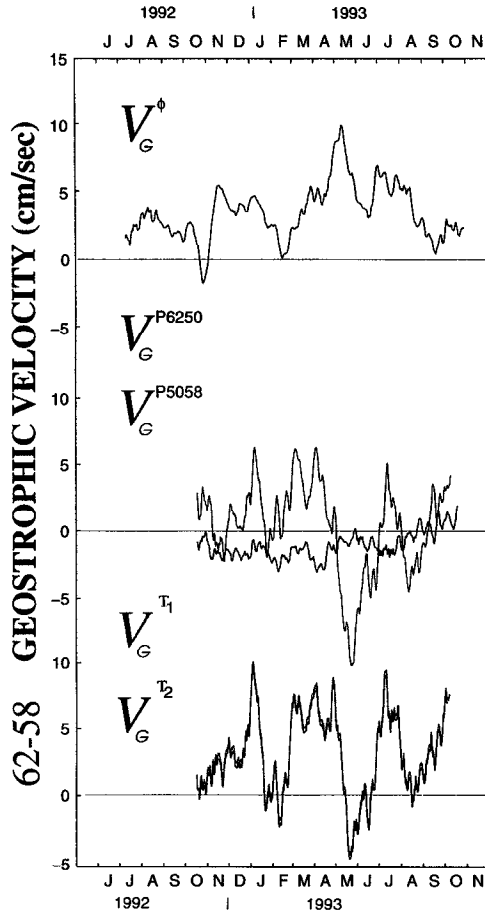


Figure 11. Geostrophic velocity as a function of time for station pairs 58 and 62: (top) baroclinic component of the geostrophic velocities, at the surface referenced to 2600 m, from the difference in  $f$ ; (middle) barotropic component of the geostrophic velocity from the difference in pressure, obtained between stations 58–50, between stations 50–62; (bottom) total geostrophic velocity at the surface from method 1 (darker line) superimposed on the geostrophic velocity from method 2 (thinner line).

However, the percentage of the total flow that this component represents is different. While in the eddy area it represents 50% of the total transport, it is only 25% of the total flow in the region of steady flow. The strong signature of the eddy in the barotropic field can be also observed in the pressure series (Fig. 9). At the location of PIES 58 there is a depression in the series during the month of May 93 that is associated with the eddy observed at that location (Clement and Gordon, 1995). Also, a depression is observed in the pressure record at IES 61 (Fig. 9), similar to the one previously associated to the passage of an eddy. This confirms previous results that suggested that the Agulhas eddies have a strong barotropic

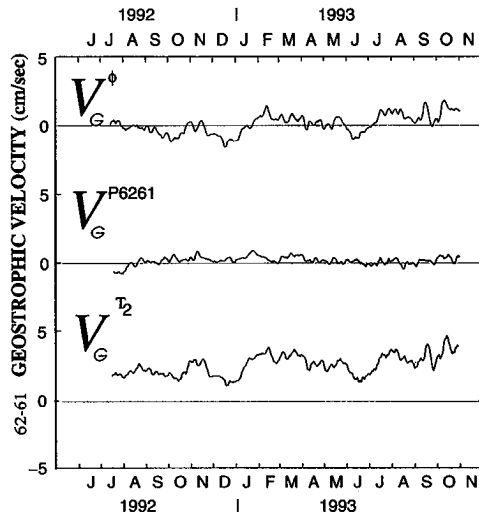


Figure 12. Geostrophic velocity as a function of time for station pairs 61 and 62, method 2.



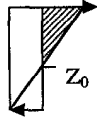
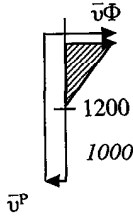
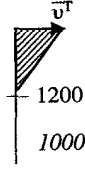
component (Kamenkovich *et al.*, 1996; Olson *et al.*, 1986; Byrne *et al.*, 1995; Clement and Gordon, 1995).

When both components are added, the total transport carried by the Benguela Current is 15 Sv. Therefore, a comparison with previous results will give an indication of the validity of the assumption that a level of no motion may be set at 1000 m. To do that, we use the results calculated with method 2 in which the transport is obtained assuming that the total velocity decreases linearly with depth up to the reference level, and determine what this level should be to obtain the same results as with method 1. The depth of the reference levels is 800 m for the eastern side of the section and 1800 m for the western side of the section. These results appear in contradiction with the notion that where the eddies are, the level of no motion should be near the bottom, while in the steady flow it will be more associated with the base of the thermocline. This apparent contradiction can be explained if it is taken into consideration that the results presented here are the mean (over a year period) transports. The rotational flow associated with the eddy field cancel; and the resultant flow is associated with the only Lagrangian displacement.

Table 5. Statistics on total geostrophic velocities in cm/s.

Station pair		Min	Max	Mean	SD
(58-61)	Method 1	-9.5	10.9	1.2	3.71
	Method 2	-9.2	11.2	1.5	3.7
62-58	Method 1	-3.0	9.1	2.8	2.2
	Method 2	-2.3	9.7	3.4	2.2
62-61	Method 2	-0.4	5.3	2.6	0.8

Table 6. Near transports obtained from the total velocities. See text for explanation.

	58-61	62-58	62-61
<i>Method 1</i>			
$T_r^\Phi \Big _{2600}^0$ 	11 Sv	25 Sv	N/A
$T_r^P \Big _{2600}^0$ 	-10 Sv	-11 Sv	N/A
Net 	1 Sv $z_0 = 800$ m	14 Sv $z_0 = 1800$ m	N/A
$T_r^{\text{Total}} \Big _{1000}^{1200}$ 	4 Sv	12 Sv	N/A
		16 Sv	
	3 Sv	10 Sv	
		13 Sv	
<hr/>			
<i>Method 2</i>			
$T_r^{\text{Total}} \Big _{1000}^{1200}$ 	4.5 Sv	11.5 Sv	17 Sv
		16 Sv	
	4 Sv	10 Sv	14 Sv
		14 Sv	

A crude extrapolation of the mean meridional velocities obtained with the current meters at sites 4 and 2 yields a zero level of 900 m at CMM4 and 2500 m at CMM2. Due to the sparse vertical resolution, these results are uncertain but they point in the same direction of those obtained with the pressure sensors.

It is interesting to note that, when the reference level is chosen as 1000 m, there is no difference in the results: The baroclinic transport across 30S obtained by Garzoli and Gordon (1996) was 13 Sv, and this value is similar to the one obtained in the first part of this paper. The total transport in the upper 1000 m obtained by method 1 is also 13 Sv and with method 2, 16 Sv when calculated from the individual pairs as well as when calculated between the 2 extreme stations. Between the limits of the errors, all these values are the same: between 13 to 14 Sv. The total geostrophic transport up to 2600 m is, according to Table 6, about 15 Sv. This corroborates the fact that in the mean, when eddies are averaged out, in the upper layer the dominant flow is the baroclinic.

## 6. Summary

The BEST experiment was designed to determine the sources of the Benguela Current and measure its transport. Both objectives were largely achieved. The main result of this paper is that it was possible to calculate the total transport of the upper 2600 m of the ocean without making any assumption about the level of no motion. And the results from this calculation corroborated the assumption that 1000 m as a level of no motion could be used as a fairly good approximation.

Unfortunately the data set collected was not sufficient to derive any conclusions about the flow below 2600 m. However, the flow below 2600 m can be assumed to be a small contribution to the time mean Benguela transport.

For many years it was thought that the Benguela transport across 30S was approximately 20 to 25 Sv. All these values were mainly derived from snapshots obtained during hydrographic cruises. During BEST it was possible to determine that this transport is typical of the Current only when an eddy is present. The analysis of the time series indicate that the annual mean transport of the Benguela Current is lower. When only the baroclinic component of the flow is considered, then in the mean the transport is approximately 13 Sv. If both barotropic and baroclinic components are considered, then this value increases up to 16 Sv.

The Benguela Current is not stationary. It is composed of a stationary flow and a transient flow, both equally important. It appears as if the stationary flow is mostly confined along the African Continent while a transient flow, composed of large eddies shed from the Agulhas retroflection, composes the western portion of the flow. In the stationary part of the Benguela Current, both barotropic and baroclinic components are equally important, while in the transient part, the barotropic is more substantial. This corroborates previous results that indicate that these eddies are strongly barotropic.

The velocity and transport series indicate a large variability. Larger variability is observed due to the passage of eddies. Several eddies were observed during the experi-

ment. These eddies translate to the west with speeds that are also higher than previous estimates obtained in the basin. They start with a speed of 12 km/day but close to the Walvis Ridge it has already diminished to 6 to 7 km/day. Again, these estimates are the same when calculated from the different data sets and with different methods. It can be assumed that after crossing the Walvis Ridge, (due to their strong barotropic component they feel the bottom) the speed decreases to that previously calculated from GEOSAT data: 1 to 5 km/day. Not all of the eddies that enter the Cape Basin area translate into the Atlantic over the Walvis Ridge. The present study suggests that only one third of the eddies that are detached from the Agulhas retroflection deviates toward the west, south of the Ridge.

The time series collected with the IES moorings indicated a recoil effect in which the thermocline appears to shallow considerably after the passage of an eddy before relaxing to the local mean. This effect is also observed and corroborated in the temperature series collected with the current meter moorings. This effect can be attributed to a small cyclonic vortex that always accompanied an anticyclonic eddy.

The sources of the Benguela Current may include Indian and South Atlantic subtropical thermocline water; the relatively saline, low oxygen tropical Atlantic water; and the cooler fresher subantarctic water. The South Atlantic thermocline and subantarctic inflow is derived from the eastward flowing South Atlantic Current. The Indian Ocean water is injected into the Benguela Current through the Agulhas retroflection eddy and filament processes. A complex stirring effect of contrasting water types is envisioned.

An interesting result is derived from the comparison between the transport associated with the Benguela Current and the salinity at the thermocline level. The changes in thermocline salinity correlate with transport: in general, when the northward transport is increasing the thermocline salinity also increases. This indicates that the Benguela Current increases in strength by bringing in more subtropical water. As the Agulhas input is most effective in boosting the salinity of the upper thermocline (the South Atlantic Current water being deficient in salinity relative to the Indian Ocean source) we suggest that the spatial variations in transport are tied to Agulhas water influx, presumably associated with the eddy field.

*Acknowledgments.* The authors are indebted to the crews of the R/V *Africana*, *Discovery* and *M. Ewing* for their invaluable collaboration during the cruises. A. Martino was in charge of the computer work associated with IES/PIES data reduction, analysis and graphics. M. Colwell assisted with the preparation of cruises and of the manuscripts for publication. BEST field work was funded by a grant from the NSF (OCE 91-02722). The data analysis is supported by NSF grant OCE 94-01950 and NOAA UCSIO P.O. 10058161, a grants/cooperative agreement from the National Oceanic and Atmospheric Administration. The views expressed herein are those of the author(s) and do not necessarily reflect the views of NOAA or any of its subagencies. This is Lamont Doherty Earth Observatory contribution number 5558.

## APPENDIX A

1. From the temperature series collected with the two current meters deployed at the top of the mooring (approximately 210 and 512 m; Table 1) the depth of the 10°C isotherm

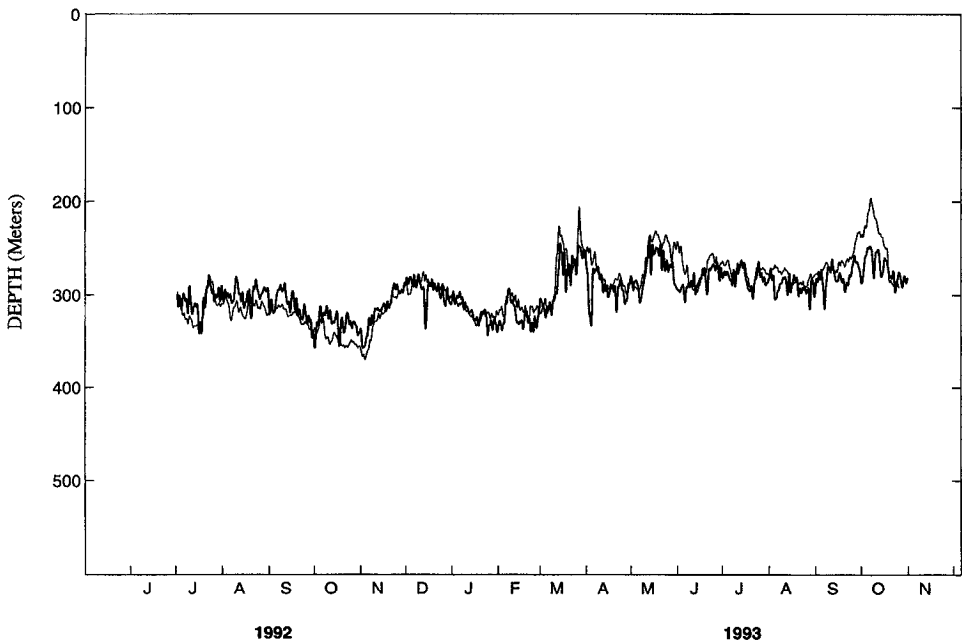


Figure A1. Comparison of the series of the depth of the 10°C isotherm, used as a proxy for the depth of the thermocline, obtained from PIES62 (thick line) and CMM1 (thinner line).

(D10°C) was determined through a linear interpolation of the data. In the event that the depth of the 10°C isotherm was lower than the depth at which the second sensor was deployed, the depth of higher isotherm (11° or 12°C) was obtained. The accuracy of the interpolation is tested by comparing the results obtained at CMM1 and PIES63. These two instruments were deployed very close to each other (23.3 km, Fig. 1) and the main variability of the series should compare. Results of the intercomparison between the depth of the 10°C isotherm obtained from the linear interpolation of the temperature series at CMM1 and that obtained at PIES 62 using a linear relation between travel time and D10°C are given in Figure A1. The series obtained with both methods are very similar. The small differences observed can be attributed to the fact that the moorings were deployed 23.3 km apart. On the basis of this agreement, series of D10°C isotherm are obtained at the location of the other three CMM: CMM 2, 3 and 4 (Fig. 1). Results are shown in Figure 3.

2. Using all the CTD casts obtained during the three BEST cruises, a relation between D10°C and the dynamic height of the surface relative to 1000 m is obtained:

$$\Delta DH(\text{dyn m}) = 9.48 \times 10^{-4} \Delta D10^\circ\text{C} (\text{m})$$

with a coefficient of correlation  $r = 0.93$  ( $r^2 = 0.87$ ) and an error of the estimate,  $\epsilon = \pm 0.047$  dyn m.

Similar regressions are obtained for the depths of the 11° and 12°C isotherms to be used

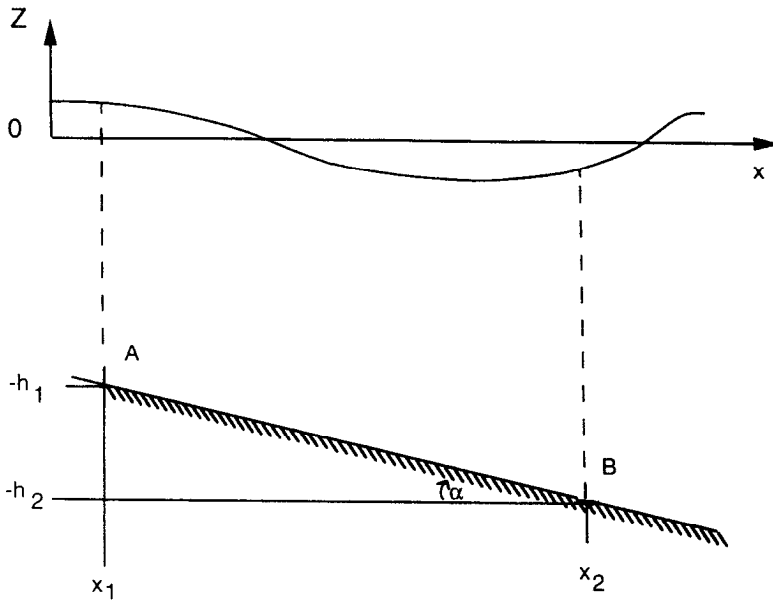


Figure B1. Schematic of the model used to calculate the geostrophic velocities from the PIES data.

in the rare cases where the D10°C surfaces:

$$\Delta DH(\text{dyn m}) = 1.00 \times 10^{-3} \Delta D11^\circ\text{C} (\text{m})$$

coefficient of correlation  $r = 0.94$  ( $r^2 = 0.88$ ); error of the estimate,  $\epsilon = \pm 0.044$  dyn m/m.

$$\Delta DH(\text{dyn m}) = 1.05 \times 10^{-3} \Delta D12^\circ\text{C} (\text{m})$$

coefficient of correlation  $r = 0.93$  ( $r^2 = 0.87$ ); error of the estimate,  $\epsilon = \pm 0.045$  dyn m/m. Figure 4 shows the time latitude variability of the dynamic series obtained through this procedure.

#### APPENDIX B

To explain the calculation of the barotropic component consider the deployment of 2 PIES at points  $A(x_1, y, -h_1)$  and  $B(x_2, y, -h_2)$  (see Fig. B1). The barotropic component of the total geostrophic velocity at the level  $z = -h_1$  is:

$$v_g^p = \frac{1}{\rho_0 f} \frac{\partial p}{\partial x} \Big|_A. \quad (\text{B.1})$$

There are no data to calculate  $(\partial p / \partial x)_A$  directly. Using the available pressure data, only  $(\partial p / \partial s)_A$  can be calculated, where  $s$  is directed along  $AB$ . Theoretically  $(\partial p / \partial x)_A$  can be

calculated from the formula:

$$\left(\frac{\partial p}{\partial s}\right)_A = \left(\frac{\partial p}{\partial x}\right)_A \cos \alpha - \left(\frac{\partial p}{\partial z}\right)_A \sin \alpha \quad (\text{B.2})$$

but simple estimates show that it is practically impossible to do so. Supposing that the geostrophic velocity  $V_g$  at  $A$  is equal to 5 cm/s, gives

$$\left(\frac{\partial p}{\partial x}\right)_A = \rho_0 f v_g \cong 10^3 \frac{\text{kg}}{\text{m}^3} \cdot 10^{-4} \text{ s}^{-1} \cdot 0.05 \frac{\text{m}}{\text{s}} = 5 \cdot 10^{-3} \text{ Pa} \cdot \text{m}^{-1} = 5 \cdot 10^{-7} \text{ db} \cdot \text{m}^{-1}$$

The value of  $(\partial p/\partial z)_A = g\rho$  is approximately  $10 \cdot 10^3 \text{ Pa} \cdot \text{m}^{-1} = 1 \text{ db} \cdot \text{m}^{-1}$ . If from the beginning the disturbance of the density  $\rho - \rho_0$  is introduced, which is on the order of  $1 \text{ kg m}^{-3}$ , and  $p$  as the deviation from the hydrostatic pressure  $p_0 = p_a - g\rho_0 z$  is understood ( $p_a$  is the atmospheric pressure), the order of this term can be reduced to  $10^{-3} \text{ db} \cdot \text{m}^{-1}$ , still three or four orders higher than  $(\partial p/\partial x)_A$ . It is clear that the order of  $(\partial p/\partial s)_A$  will be also of  $10^{-3} \text{ db} \cdot \text{m}^{-1}$ . Thus, to calculate  $(\partial p/\partial x)_A$  from (B.2),  $p$  and  $\rho$  would have to be measured with unrealistic accuracy, not provided by the present instruments.

Therefore the procedure is as follows. The time variable parts of terms in (B.1) are considered by removing the corresponding time means.

$$v'_g = \frac{1}{\rho_0 f} \frac{\partial p'}{\partial x} \Big|_A \quad (\text{B.3})$$

where  $'$  denotes the deviation from a time mean. For the variable part of the pressure

$$p'(x_2, y, -h_1, t) = p'(x_2, y, -h_2, t) - \int_{-h_2}^{-h_1} g\rho'(x_2, y, z, t) dz \quad (\text{B.4})$$

is obtained.

Now the fact is taken into consideration that temporal variations of the density  $\rho'$  at great depths are very small and can therefore be neglected. Hence

$$p'(x_2, y, -h_1, t) = p'(x_2, y, -h_2, t) \quad (\text{B.5})$$

Using (B.5) the right-hand side of (B.3) is easily calculated. An attempt has been made to estimate the second term on the right-hand side of (B.4) using CTD BEST stations at PIES station 58. The following formula is applied.

$$J = g \int_{-h_2}^{-h_1} (\rho - \rho_0) dz = 10^4 \cdot \int_{p_1}^{p_2} \frac{\rho(T, S, p) - \rho(0, 35, p)}{\rho(T, S, p)} dp \quad (\text{B.6})$$

where  $p$  is in decibars, the SI system is used for all other variables, and  $\rho_0 = \rho(0, 35\text{‰}, p)$ . Results are shown in Table B1. The mean of  $J$  is  $-0.8813 \text{ db}$ . Then the deviations are:  $-0.0187 \text{ db}$ ,  $+0.0236 \text{ db}$ , and  $-0.0049 \text{ db}$ . Or, in other words, the time variations of  $J$  are less than 20%. Therefore  $J'$  can be neglected. It is important to stress that (B.5) can be



Table B1.

	Date	$h_1$ , km	$h_2$ , km	$J$ , db
BEST 1	6/23/92	3.023	5.123	-0.9000
BEST 2	5/11/93	3.022	5.122	-0.8577
BEST 3	10/29/93	3.023	5.122	-0.2862

interpreted as the  $z$ -independence of the time-variable part of the pressure. This statement is true, of course, below a certain depth.

## REFERENCES

- Belinne, J. D., P. Mele and B. Huber. 1996. CTD and Hydrographic data from BEST 2 cruise, 1993, Lamont-Doherty Data Report 96-1.
- Broecker, W. S. 1991. The great ocean conveyor belt. *Oceanogr.*, 4, 79–89.
- Byrne, D. A., A. L. Gordon and W. F. Haxby. 1995. Agulhas eddies: A synoptic view using Geosat ERM data. *J. Phys. Oceanogr.*, 25, 902–917.
- Chiswell, S. M., D. R. Watts, and M. Wimbush. 1986. Using inverted echo sounders to measure dynamic height in the eastern equatorial Pacific during the 1982–83 El Niño. *Deep-Sea Res.*, 33, 981–991.
- 1987. Inverted echosounders observations of variability in the eastern equatorial Pacific during the 1982–83 El Niño. *Deep-Sea Res.*, 34, 313–327.
- Clement, A. and A. L. Gordon. 1995. The absolute velocity field of Agulhas eddies and the Benguela Current. *J. Geophys. Res.*, 100 (C11), 22,591–22,601.
- Duncombe-Rae, C., S. L. Garzoli and A. L. Gordon. 1996. The eddy field of the South-East Atlantic Ocean: A Statistical Census from the BEST Project. *J. Geophys. Res.*, 101 (C5), 11,949–11,964.
- Garzoli, S. L. and A. L. Gordon. 1996. Origins and Variability of the Benguela Current. *J. Geophys. Res.*, 101 (C1), 897–906.
- Garzoli, S. L., A. L. Gordon and D. Pillsbury. 1994a. Initial results in from BEST Cruises. WOCE Notes, 6, 10–11, 15.
- Garzoli, S. L., M. Maccio, A. Martino and M. Colwell. 1994b. BEST Data Report, IES/PIES/XBT Data, Lamont-Doherty Earth Observatory Data Report, LDEO-94-1.
- Gordon, A. L. 1981. South Atlantic thermocline ventilation. *Deep-Sea Res.*, 28, 1239–1264.
- 1985. Indian Atlantic transfer of thermocline water at the Agulhas retroflection. *Science*, 222, 1030–1033.
- Gordon, A. L. and W. F. Haxby. 1990. Agulhas eddies invade the South Atlantic: evidence from Geosat altimeter and ship-board Conductivity-Temperature-Depth survey. *J. Geophys. Res.*, 95 (C3), 3117–3125.
- Gordon, A. L., J. R. E. Lutjeharms and M. L. Gründlingh. 1987. Stratification and circulation at the Agulhas retroflection. *Deep-Sea Res.*, 34, Part A, 565–599.
- Gordon, A. L., R. F. Weiss, W. M. Smethie and M. J. Warner. 1992. Thermocline and intermediate water communication between the South Atlantic and Indian Ocean. *J. Geophys. Res.*, 97, 7223–7240.
- Hooker, S. B. and J. W. Brown. 1994. Warm core ring dynamics derived from satellite imagery. *J. Geophys. Res.*, 99 (C12), 25,181–25,234.
- Kamenkovich, V. M., Y. P. Leonov, D. A. Nechaev, D. A. Byrne and A. L. Gordon. 1996. On the influence of bottom topography on the Agulhas eddy. *J. Phys. Oceanogr.*, 26, 892–912.
- Lutjeharms, J. R. E. 1981. Features of the southern Agulhas Current circulation from satellite remote sensing. *S. Afr. J. Sci.*, 77, 231–236.

- Lutjeharms, J. R. E. and J. Cooper. 1996. Inter-basin leakage through Agulhas Current filaments. *Deep-Sea Res.*, 43, 213–238.
- Lutjeharms, J. R. E. and A. L. Gordon. 1987. Shedding of an Agulhas ring observed at sea. *Nature*, 325, 138–140.
- Lutjeharms, J. R. E. and R. C. van Ballegoyen. 1988. The retroflection of the Agulhas Current. *J. Phys. Oceanogr.*, 18, 1570–1583.
- Lutjeharms, J. R. E. and D. J. Webb. 1995. Modeling the Agulhas Current System. *Deep-Sea Res.*, 42, 523–551.
- McWilliams, J. C. and G. R. Flierl. 1979. On the evolution of isolated, nonlinear vortices. *J. Phys. Oceanogr.*, 9, 1155–1182.
- Mied, R. P. and G. J. Lindemann. 1979. The propagation and evolution of cyclonic Gulf Stream rings. *J. Phys. Oceanogr.*, 9, 1183–1206.
- Olson, D. B. and R. H. Evans. 1986. Rings of the Agulhas Current. *Deep-Sea Res.*, 33 (1A), 27–42.
- Olson, D. B., R. A. Fine and A. L. Gordon. 1992. Convective modification of water masses in the Agulhas. *Deep-Sea Res.*, (Suppl. 1), S163–S181.
- Pillsbury, R. D., J. M. Bottero, G. Pittock, D. C. Root, J. Simpkins, III and R. E. Still. 1994. Benguela Source and Transport Project (BEST): Current measurements off the coast of South Africa. WOCE ACM-4. June 1992–October 1993. COAS, Oregon State University, Data Report 157, 69 pp.
- Reid, J. L. 1989. On the total geostrophic circulation of the South Atlantic Ocean: Flow patterns, tracers and transports. *Progr. Oceanogr.*, 23, 149–244.
- Schmitz Jr., W. J. 1995. On the interbasin-scale thermohaline circulation. *Rev. Geophys.*, 33, 151–173.
- Shannon, L. V., J. R. E. Lutjeharms and J. J. Agenbag. 1989. Episodic input of subantarctic water into the Benguela region. *S. Afr. J. Sci.*, 85, 317–322.
- Smythe-Wright, D., A. Gordon and P. Chapman. 1996. CFC shows Brazil Current Rings crossing the South Atlantic to the Agulhas Retroflection Region. *J. Geophys. Res.* 10, 885–895.
- Stramma, L. and R. G. Peterson. 1989. Geostrophic Transport in the Benguela Current Region. *J. Phys. Oceanogr.*, 19, 1440–1448.
- van der Berg, R. E. 1992. Chemical Physical Section Cruise Data of Cruise No. OA105, *FRS Africana*, South Africa Sea Fisheries Research Institute, Internal Report, Cape Town.
- Wimbush, M., S. M. Chiswell, R. Lukas and K. A. Donohue. 1990. Inverted echosounder measurements of dynamic height through an ENSO cycle in the central Equatorial Pacific. *IEEE J. Ocean Eng.*, 15, 380–383.